NANO LETTERS

2005
Vol. 5, No. 7
1303−1307

Approaching the Resolution Limit of Nanometer-Scale Electron Beam-Induced Deposition

Willem F. van Dorp, Bob van Someren, Cornelis W. Hagen,* and Pieter Kruit

Delft University of Technology, Faculty of Applied Sciences, Lorentzweg 1, 2628 CJ Delft, The Netherlands

Peter A. Crozier

Center for Solid State Science, Arizona State University, Tempe, Arizona 85287

Received March 18, 2005

ABSTRACT

We report the writing of very high resolution tungsten containing dots in regular arrays by electron beam-induced deposition (EBID). The size averaged over 100 dots was 1.0 nm at fwhm. Because of the statistical spread in the dot size, large and small dots are present in the arrays, with the smallest having a diameter of only 0.7 nm at fwhm. To date these are the smallest features fabricated by EBID. We have also fabricated lines with the smallest having a width at fwhm of 1.9 nm and a spacing of 3.2 nm.

Electron beam-induced deposition (EBID) is a process in which an electron beam is focused on a substrate surface onto which precursor gas molecules are adsorbed. Because of inelastic collisions of the incoming (primary) electrons, secondary electrons (SEs) are generated in the substrate, some of which have sufficient energy to be re-emitted from the surface. Their energies are close to where the precursor dissociation cross section has a peak (typically 20−50 V); therefore, the SEs are most likely to dissociate the precursor molecules in or close to the irradiated area. Nonvolatile products of this process adhere to the substrate, and as a result, a deposit grows in the irradiated area. The composition of the deposit depends on the type of precursor.

Resist-based electron beam lithography can currently achieve a resolution of about 10 nm.[1] EBID can go beyond that resolution because modern electron microscopes are capable of bringing the electron beam diameter down to tenths of a nanometer. EBID allows the fabrication of structures for nanoscale research, and perhaps the technique is suitable to continue Moore's law[2] into the sub-10-nm regime. Although the resolution of scanning probe lithography techniques is unsurpassable, they have the inherent problem of being limited in speed. EBID has a better prospect regarding speed even though it also has its limitations, but apart from that, it is interesting to determine the ultimate resolution limit of the technique. We have built a Monte Carlo simulation to study the influence of the substrate−electron beam interaction on the resolution of EBID.[3] The model predicted that a small electron beam in combination with a short illumination time would allow the writing of sub-10-nm structures. This was demonstrated successfully in a scanning transmission electron microscope (STEM) using contamination as a precursor.[4] Although sub-10-nm structures have since been deposited using a scanning electron microscope (SEM),[5] the very small electron beams achievable in (S)TEMs have recently been used to synthesize sub-5-nm structures from a variety of precursors.[6,7] The smallest nanodot from which an image was published was a single dot of about 1.5 nm deposited from $W(CO)_6$, the diameter being estimated from a slightly overfocused high-resolution TEM image.[7] This result was established in an ultrahigh vacuum TEM using a very low precursor pressure of 2×10^{-6} Pa (1.5×10^{-8} Torr) and a 1-nm-diameter beam. Sub-10-nm lines containing metal have been written by Jiang et al.[8] and Shimojo et al.[9] However, at present there remain many questions about the ultimate experimental limits that can be achieved in nanostructures fabricated using EBID. Here we perform experiments that explore the resolution limits of EBID for the fabrication of a variety of nanostructures. We demonstrate the capabilities of EBID as a resistless high-resolution patterning technique and show that this approach can be used to synthesize structures as small as 1.0 nm.

Nanolithography and characterization were conducted in a Tecnai environmental TEM, allowing the entire growth process to be observed and controlled in situ and in real time.

* Corresponding author. E-mail: c.w.hagen@tnw.tudelft.nl.

10.1021/nl050522i CCC: $30.25
Published on Web 06/07/2005

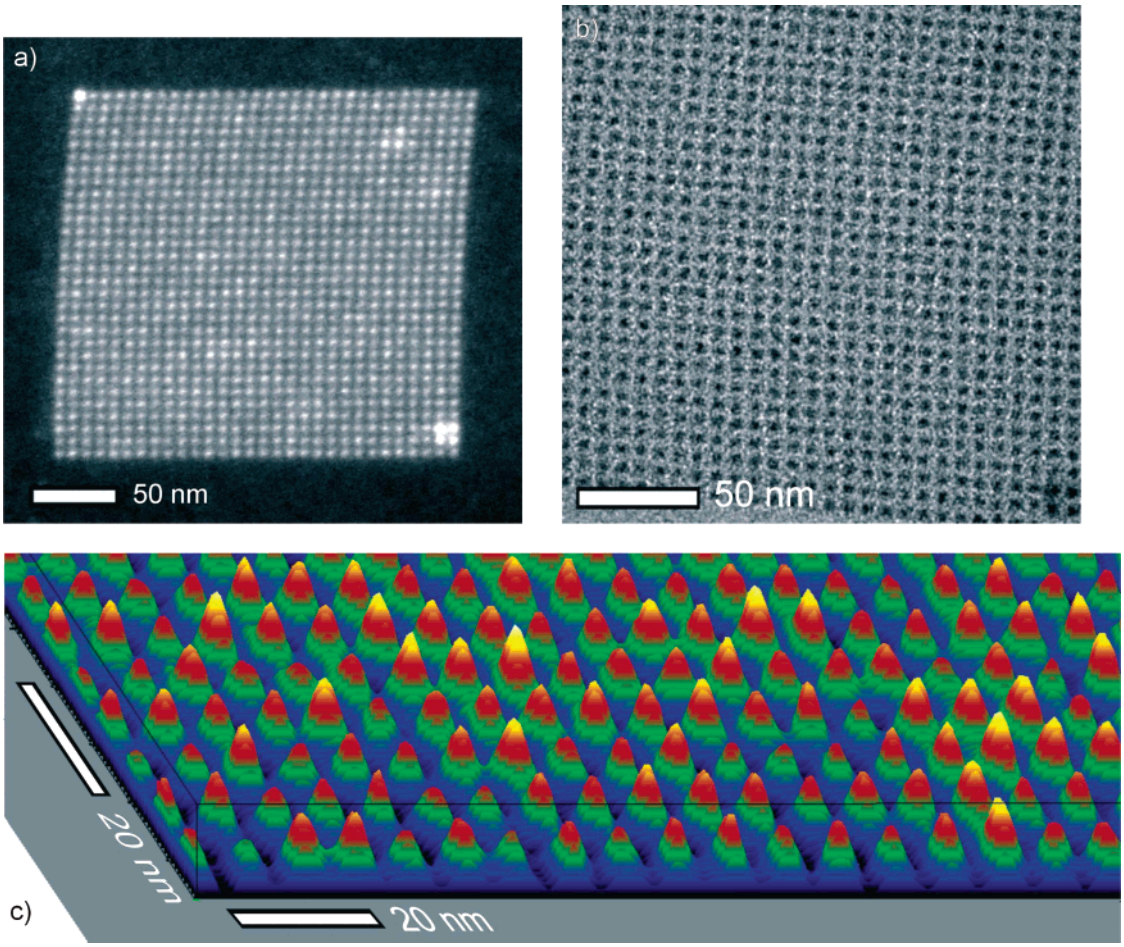

Figure 1. (a) ADF image of an array of dots deposited from $W(CO)_6$. (b) TEM image of the same array at best focus to show the dots. (c) 3D intensity plot of a part of the ADF image.

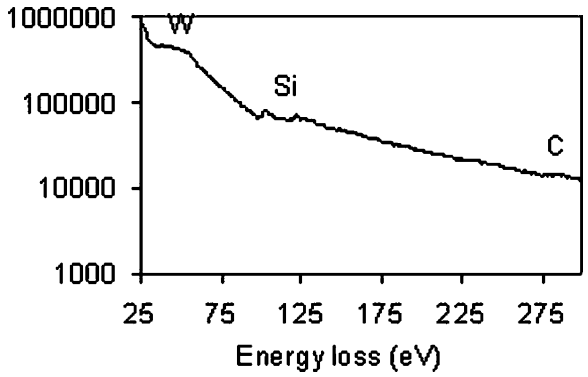

Figure 2. Energy-loss spectrum from the deposited dot showing the presence of W. The spectrum shows a W $N_{67}O_{23}$-edge at 40−50 eV, a Si L-edge at 100 eV (from underlying Si_3N_4 substrate) and a C K-edge at 284 eV.

This 200 kV microscope is equipped with a field-emission electron source and was operated in STEM mode with a nominal beam spot size of 0.3 nm with a current of approximately 40 pA. The microscope is fitted with an environmental cell allowing gas pressures of up to 8 Torr in the sample chamber during observation. The precursor used for deposition was $W(CO)_6$, and typical pressures were in the range of 1×10^{-3} Torr. The substrate consisted of a 30-nm-thick Si_3N_4 membrane. To reduce the effect of hydrocarbon contamination, the substrate was plasma cleaned for about 3 h in an Ar/O_2 mixture and then inserted into the

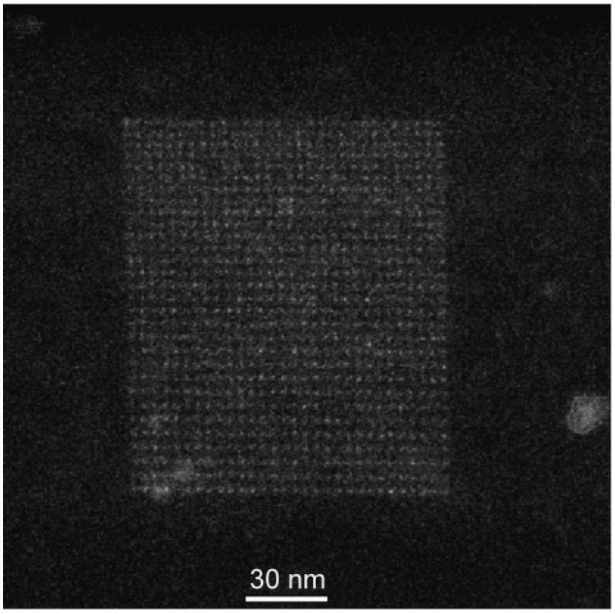

Figure 3. ADF image of a 30 × 30 array of dots spaced at 4.0 nm. A spread in dot size can be seen from the varying brightness between individual dots.

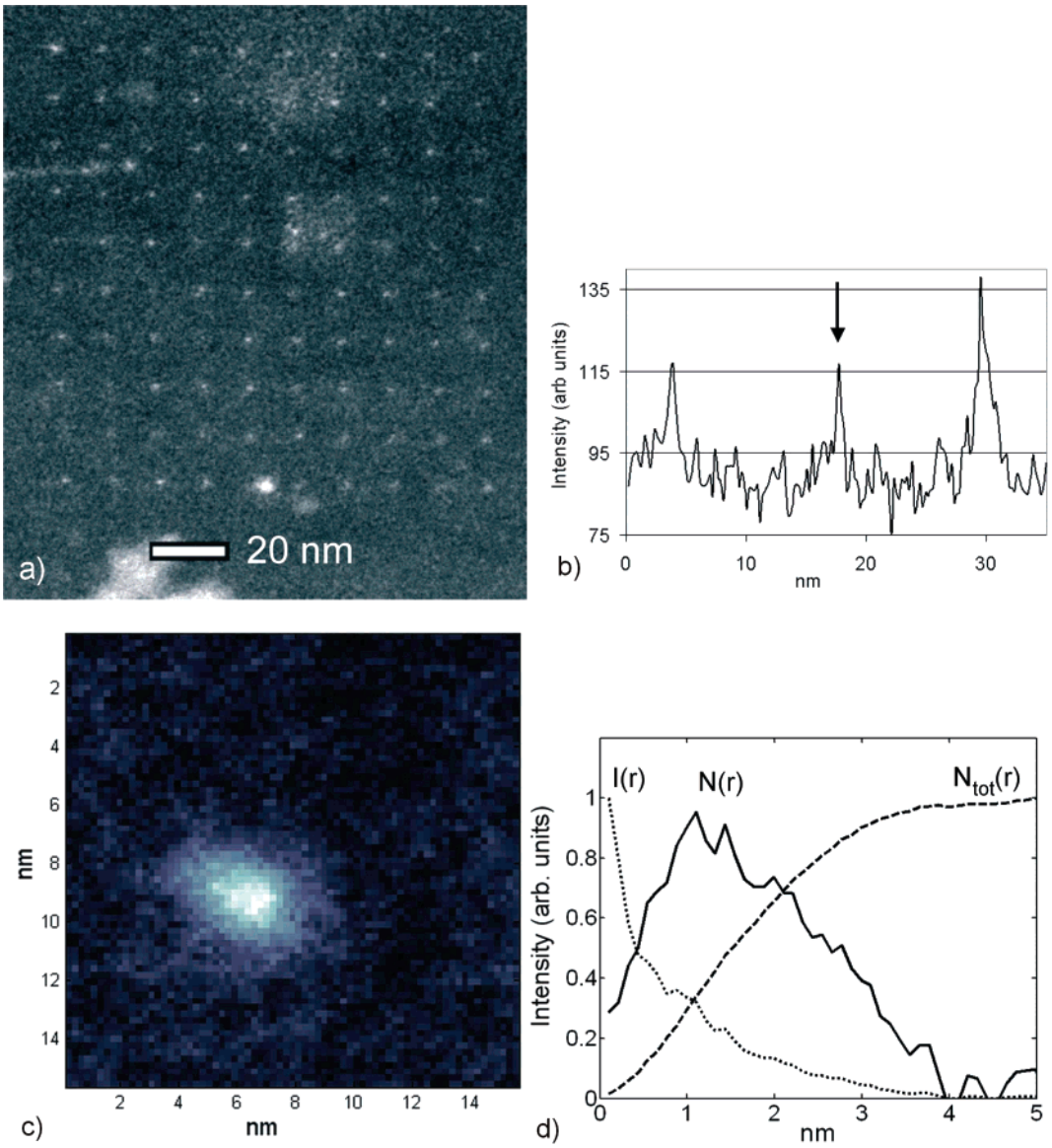

Figure 4. (a) ADF image of a 10 × 10 array of dots deposited from $W(CO)_6$, with an average diameter of 1.0 nm. The array is slightly skewed because of drift. A spread in dot size can be seen as a variation in brightness. (b) Line scan from part of the array in panel a. The smallest dot (at position (2, 8) counting from left to right, top to bottom) is 0.7 nm in diameter at fwhm and is indicated by the arrow. (c) Averaged profile of the 100 dots in panel a. (d) $I(r)$ shows the intensity in panel c as a cross section that is averaged over many directions through the dot. The diameter at fwhm is 1.0 nm. $N(r)$ is the intensity in a ring of radius (r, $r + dr$). $N_{tot}(r)$ is the integral function of $N(r)$.

microscope. Further substrate cleaning was performed in situ by heating to about 200 °C in a stream of 5% H_2 and 95% Ar for about 45 min. During experiments, the substrate was kept at a temperature of 107 °C. The spectrum imaging software present on the Tecnai microscope was used to control the electron beam location during patterning. The program allowed the deposition of dots at designated locations, but full control of the beam was not possible. The scanning of continuous lines was not possible, and instead, deposited lines were written with overlapping dots. Typical deposition times were on the order of 50−100 ms.

Most of the imaging was performed with the annular dark field (ADF) signal. This image has a strong *Z*-contrast component, and interpretation and feature size measurements are relatively straightforward compared to phase-contrast TEM. This allows the detection of very small features (single atoms in the case of heavy elements on thin parts of the specimen), and for thin films, the image contrast is linear with mass or thickness. Because the definition of size becomes important when discussing the limits of resolution, we consequently consider the fwhm measured in the ADF images.

Figure 1a shows a 30 × 30 dot array. The dots are precisely placed on the intended grid, although the array is not square because of sample drift during the serial deposition process. The average dot size taken over 30 dots is 4.0 nm at fwhm. Figure 1b shows a TEM image of a part of the array taken at the best focus to show the dots. A 3D intensity plot of the ADF image is shown in Figure 1c, with arbitrary units along the *z* axis.

Figure 2 is a typical energy-loss spectrum recorded from a larger dot and shows a strong W signal confirming that W

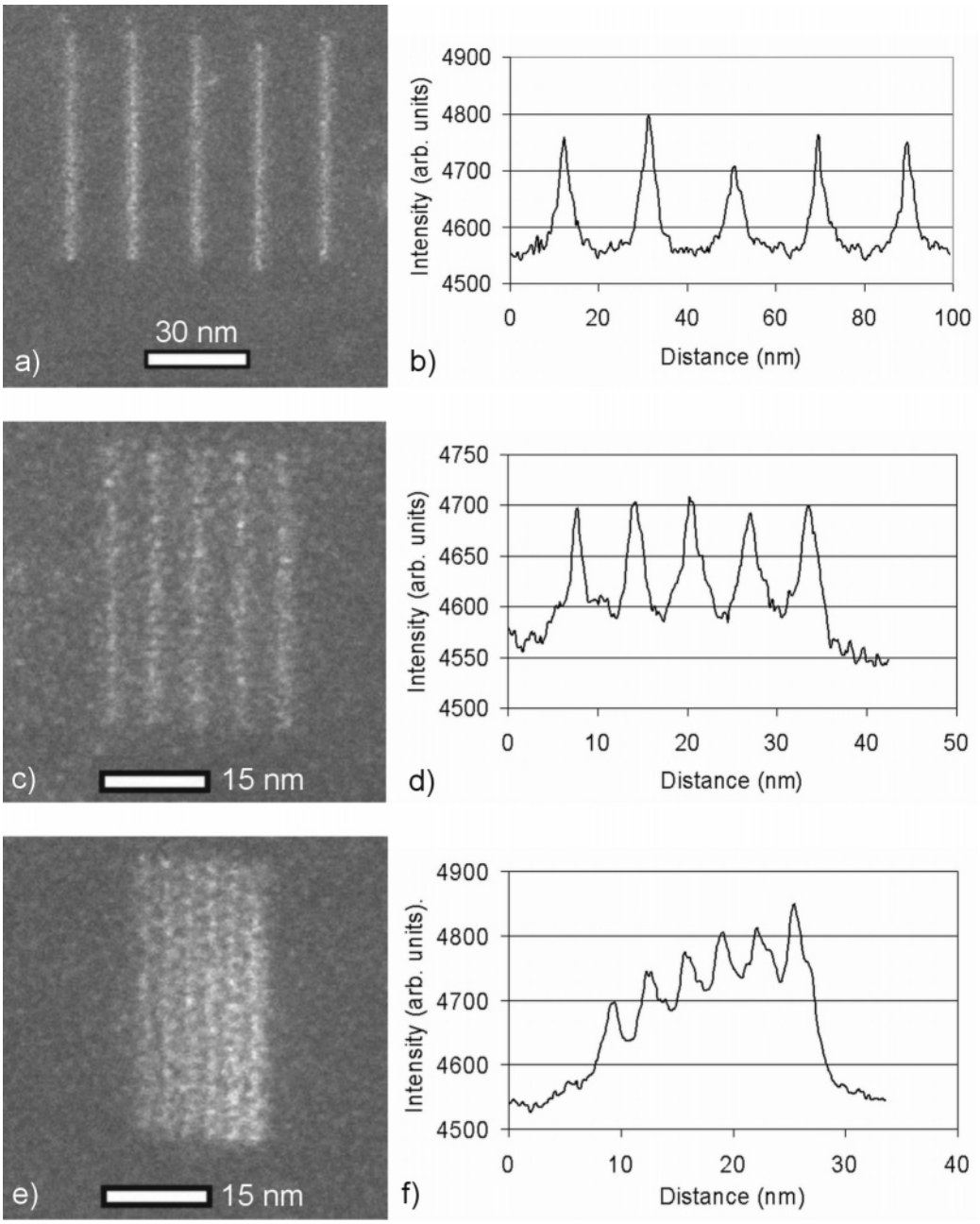

Figure 5. HAADF images of lines and spaces. Line widths for a and c are 3.2 and 1.9 nm, respectively. Spacings for a, c, and e are 19.5, 6.5, and 3.2 nm, respectively. (b, d, f) Line scans from panels a, c, and d, respectively, integrated over a length of 15 nm.

is the dominant species in the deposition. The small carbon signal present in the spectrum may be residual carbon species from the original carbonyl molecule.

A 30 × 30 dot array with smaller dots and a spacing of 4.0 nm has been fabricated (Figure 3). There is drift, making the array rectangular and slightly skewed, and the dots do not lie exactly on the intended pattern grid. There is also a spread in the dot size as can be seen in the ADF image from the varying brightness between individual dots.

The small spacing of the dots makes the measurement of the average dot size difficult; therefore, we fabricated another set with larger spacing. The 10 × 10 array in Figure 4a was fabricated under the same conditions as the array in Figure 3, except for a larger spacing of 12.9 nm. To measure the dot size, we have averaged over the 100 dots of Figure 4a by fitting a trapezoidal grid to the positions of the dots. For each grid point, a box was taken centered around the grid point, and the sum of all boxes is shown in Figure 4c. This procedure gives some widening of the average dot size because of the arbitrary placement of the dots. In Figure 4d, we plot the intensity $I(r)$ in Figure 4c as the cross section through the dot, obtained by averaging in many different directions through the dot. $N(r)$ is the intensity in a ring of radius $(r, r + dr)$. $N_{tot}(r)$ is the integral function of $N(r)$, showing the total deposited W within a circle of radius r. The plot of $I(r)$ shows a fwhm of 1.0 nm. This average dot diameter is precisely defined and to our knowledge represents a new world record for EBID. Because of the spread in the

dot size, smaller diameters than the average are found, of course, the smallest of which is only 0.7 nm in diameter (fwhm) and is indicated by the arrow in Figure 4b.

Both the variation in dot size and dot position (the arbitrary placement of the dots around the intended grid points) highlight the random nature of the deposition process on the nanometer and subnanometer length scales. Taking the volume of a single tungsten atom of 0.0158 nm^3 and assuming that the dots are half-spheres consisting of pure W and having a base diameter of 1.4 nm, the average number of atoms per dot is about 45. The spread in the number of atoms is on the order of 6 or 7 (the square root of 45). Even when the dots would contain no W at all but would consist of pure carbon the average number of atoms per dot would be 96, with a statistical spread of about 10. This variation is much larger than the expected variation in the number of electrons involved in the writing of the dot (approximately $3000/10^7$ electrons) and thus dominates the statistics. Of course, other mechanisms may also contribute to the observed spread, such as surface inhomogeneity, surface diffusion, or autocatalytic effects of the decomposition.

When discussing Moore's law, it is customary to define the resolution in terms of half pitch: the width of parallel lines separated by spacings equal to the line width. The most advanced integrated circuits are now written with a 65 nm half pitch. In Figure 5, ADF images of lines and spaces are shown, together with accompanying line scans integrated over 15 nm. Each individual line is written from top to bottom, and the series of lines are written from left to right. The lines in Figure 5a consist of 50 dots each along a 64 nm line, having a line width of 3.2 nm and a spacing of 19.5 nm. The lines in Figure 5c consist of 25 dots each along a 39 nm line, having a line width of 1.9 nm and a spacing of 6.5 nm. The lines in Figure 5e are written under the same conditions as the lines in Figure 5c, except for a smaller spacing of 3.2 nm that corresponds to a half pitch of only 1.6 nm.

The line scan in Figure 5d shows that the line bases in Figure 5c overlap because of the nonlocal emission of secondary electrons from the sample surface. On more closely spaced lines, the intensity of the line base increases with each line drawn as shown in Figure 5e and f. This is caused by the steady increase in secondary electron emission from the base as new lines are deposited. Although the first line is deposited on a flat, clean surface, the second line is deposited on the already existing base of the first line. Secondary electron generation will be enhanced because of the fact that W is already present on the irradiated area, a heavier element than Si or N. Second, when writing the second line, the surface is no longer perpendicular to the electron beam because of the presence of the base of the first line. The angle of incidence of the beam has changed, and this allows more SEs to escape from the surface and dissociate more precursor species. This process is repeated for the following four lines and results in increasing line height from left to right. Hence, the profile of the two closely spaced lines is not a linear sum of two individual lines (as is the case for the lines in Figure 5d) but rather consists of closely spaced lines superimposed on an increasing ramp.

In conclusion, we have written dots with an average fwhm of 1.0 nm that are the smallest structures made to date with the EBID approach. Under similar conditions, dots were written in an array with a spacing of 4.0 nm. The statistical spread in dot size and location becomes evident and is significant at this high-resolution writing. Also, we have written continuous lines with a fwhm of 1.9 nm, with the smallest spacing being only 3.2 nm. These experiments demonstrate that EBID is a promising technique for high-resolution resistless lithography and that the STEM is a suitable instrument for achieving the sub-5-nm regime.

Acknowledgment. We gratefully acknowledge the use of the facilities in the Center for Solid State Science at Arizona State University.

References

(1) Word, M. J.; Adesida, I.; Berger, P. R. *J. Vac. Sci. Technol., B* **2003**, *21*, L12−L15.
(2) Moore, G. E. *Electronics* **1965**, *38*, 114−117.
(3) Silvis-Cividjian, N.; Hagen, C. W.; Leunissen, L. H. A.; Kruit, P. *Microelectron. Eng.* **2002**, *61*−*2*, 693−699.
(4) Silvis-Cividjian, N.; Hagen, C. W.; Kruit, P.; Van der Stam, M. A. J.; Groen, H. B. *Appl. Phys. Lett.* **2003**, *82*, 3514−3516.
(5) Guise, O.; Ahner, J.; Yates, J.; Levy, J. *Appl. Phys. A* **2004**, *85*, 2352−2354.
(6) Crozier, P. A.; Tolle, J.; Kouvetakis, J.; Ritter, C. *Appl. Phys. Lett.* **2004**, *84*, 3441−3443.
(7) Tanaka, M.; Shimojo, M.; Han, M.; Mitsuishi, K.; Furuya, K. *Surf. Interface Anal.* **2005**, *37*, 261−264.
(8) Jiang, H.; Borca, C. N.; Xu, B.; Robertson, B. W. *Int. J. Mod. Phys. B* **2001**, *15*, 3207−3213.
(9) Shimojo, M.; Mitsuishi, K.; Tameike, A.; Furuya, K. *J. Vac. Sci. Technol., B* **2004**, *22*, 742−746.

NL050522I